E-Appendix

Details of Data Analysis

The contact stress data sets mapped continuous contact stresses over the entire articular surface (the 46 × 32 sensel grid distributed over the articular surface) for each 1/132-second time-frame, for the complete stance event. Analysis was performed on data sampled between the 40% (0.8-second) and 90% (1.8-second) time-points of the duty cycle to focus on the instability event, representing 194,304 stress measurements (1472 measurements × 132 samplings) in each test. Low-amplitude noise artifacts from the out-of-contact area (identified by stress values of <0.25 MPa) were removed with a low-pass digital filter. Also, to minimize experiment artifact due to local sensor irregularities, stress values were mask-filtered on the basis of neighboring sensel measurements. For each sensel, data from the eight adjacent sensels, representing a 3 × 3 sensel grid, were considered, and the highest six values from the nine-sensel grid were averaged, to obtain a final value at each individual sensel. The 194,304 contact stress values were rank-ordered, and the individual peak and 95th percentile values were determined for each specimen under each condition.

For each sensel at each time-point, the Lagrange formula was applied to calculate contact stress rates on the basis of contact stress data from the previous two frames and the subsequent two frames. Again, analysis of contact stress rates was performed on data measured between the 40% and 90% time-points of the testing cycle, producing 132 consecutive data sets with 1472 contact stress rates measurements, or 194,304 individual contact stress rate data points per specimen. Positive rates of stress change indicated that stress was instantaneously increasing, and, conversely, negative rates of change indicated that stress was instantaneously decreasing. Positive and negative contact stress rate values were rank-ordered, and the individual peak global positive and negative contact stress rates were determined for all conditions. To define an envelope encompassing the majority of values of contact stress rates, the 95th percentile distribution window of contact stress rates, defined by calculating the absolute difference between the 95th percentile positive and 95th percentile negative contact stress rates for each test condition, was determined.

Contact stress rates were also calculated from each specimen, under all three conditions, subjected to static loading conditions to quantify potential numerical differentiation-associated artifact introduced by calculating contact stress rate values from the raw contact stress data. Theoretically, under static loading, contact stress rates should uniformly measure zero. Specimens were held under 300 N of axial load, with the 30-N anteriorly directed stabilization force, with no motion for 0.5 second. Contact stress rates were calculated with use of the central differencing formula.

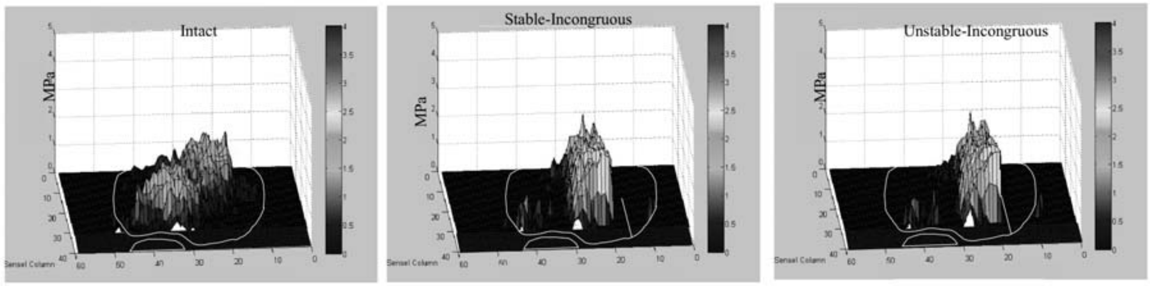

Contact Stress

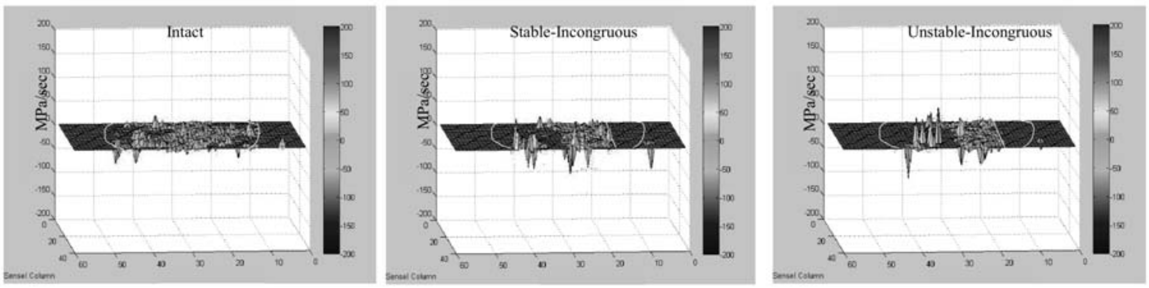

Contact Stress Rate

Fig. E1-A

Figs. E1-A through E1-D Contour plots of contact stresses and contact stress rates demonstrate feature differences between the intact, stable-incongruous, and unstable-incongruous conditions. Fig. E1-A Just prior (one sampling frame, 1/132nd of a second) to the subluxation pulse, contact stresses and contact stress rates are relatively homogeneous in all three conditions.

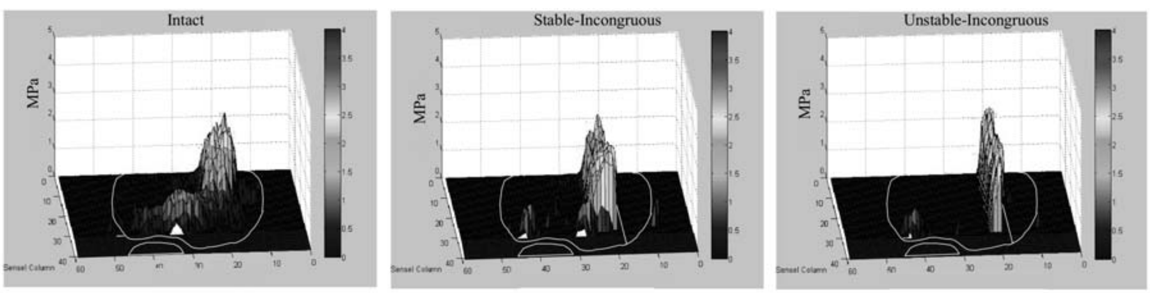

Contact Stress

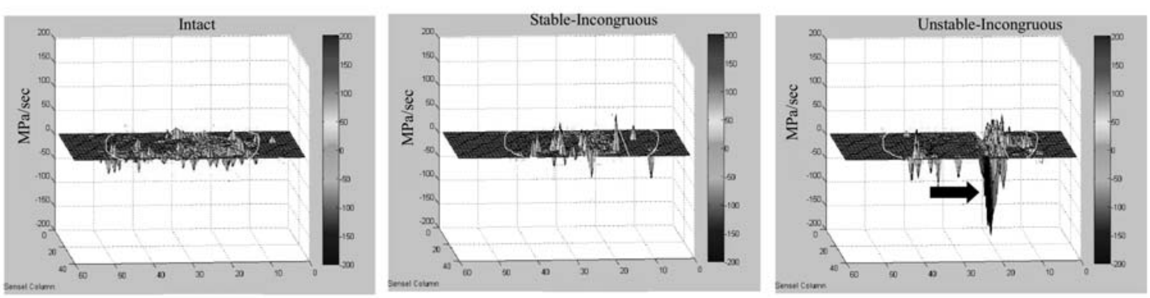

Contact Stress Rate

Fig. E1-B

At the instant of the onset of subluxation in the unstable-incongruous condition, a sharp focus of negative contact stress rate is evident along the posterior border of the osteotomy site (arrow). In contrast, stresses and stress rates are low-magnitude and homogeneous in the intact and stable-incongruous conditions at the same instant.

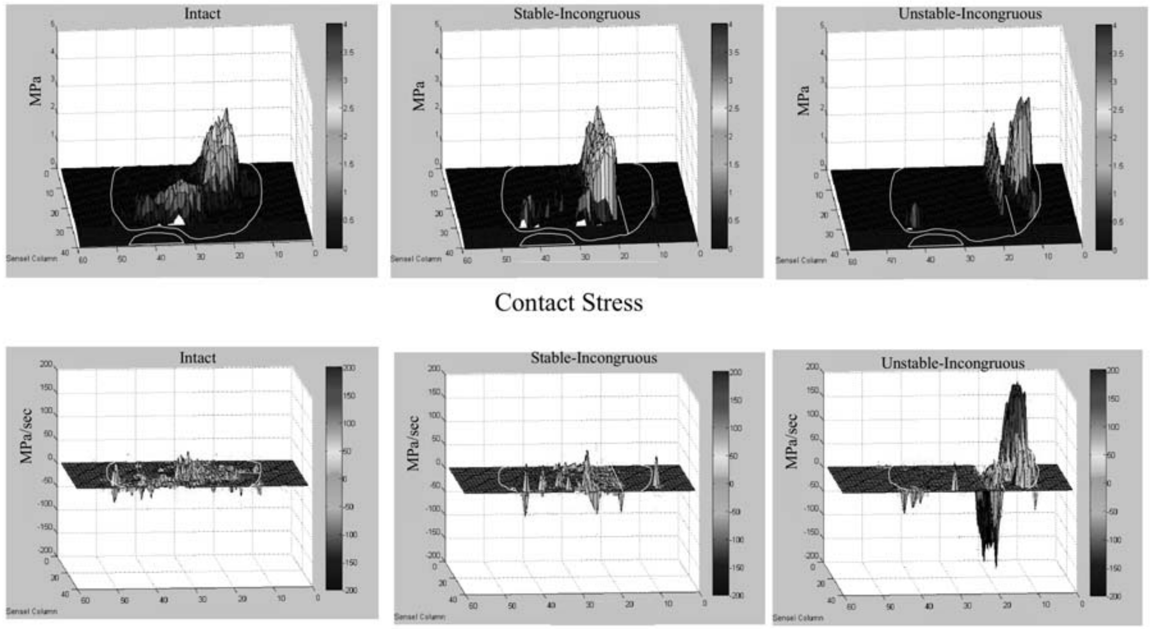

Contact Stress Rate

Fig. E1-C
At the instant of maximum subluxation, a focus of contact stress and positive stress rate on the anterior fragment with a corresponding focus of negative contact stress rate on the posterior border of the osteotomy site is evident in the unstable-incongruous condition. This occurred four to five frames (0.030 to 0.038 second) subsequent to the second time-point in all seven specimens. Contact stress rates remained low and homogeneous in the intact and stable-incongruous conditions.

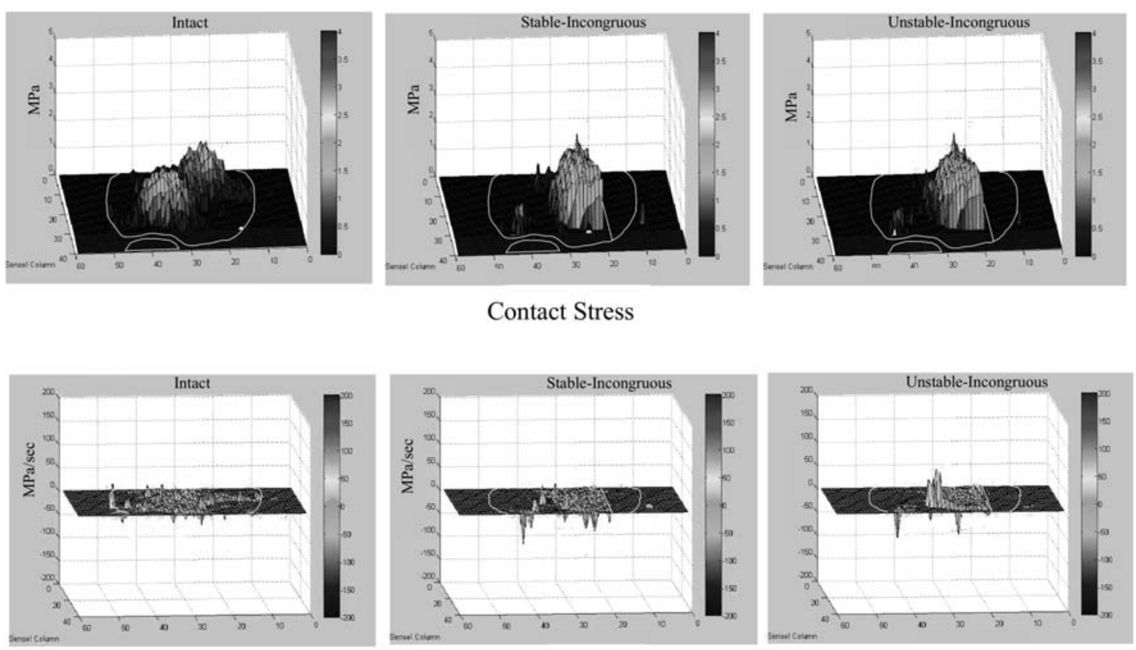

Contact Stress Rate

Fig. E1-D
After the subluxation pulse had returned to 0 N, contact stress and contact stress rates had returned to previous homogeneous low-level values in all conditions.

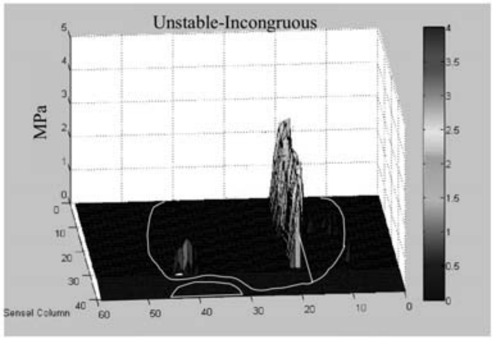

Frame 1

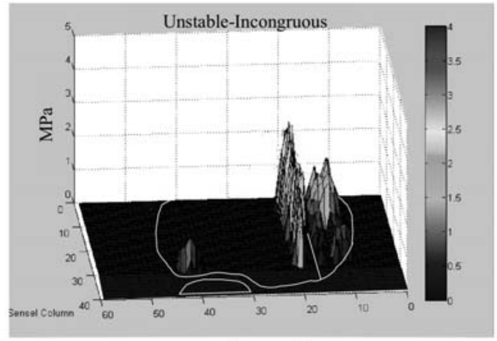

Frame 2

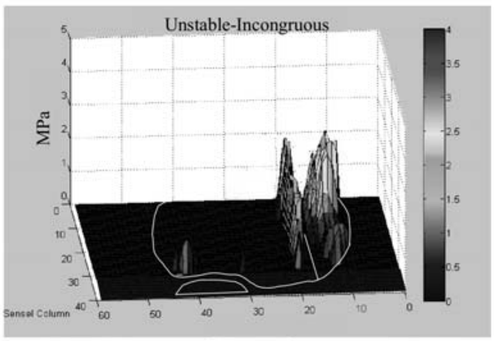

Frame 3

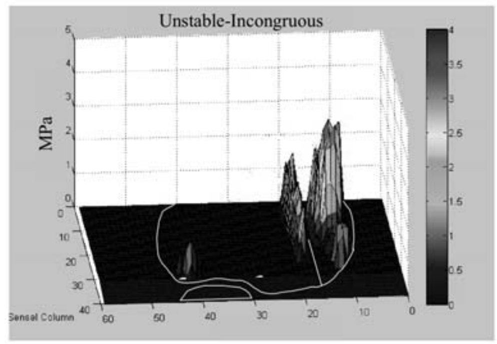

Frame 4

Fig. E2-A

Figs. E2-A and E2-B Representative contour plots of contact stresses and contact stress rates during the subluxation event in the unstable-incongruous condition. Fig. E2-A Four consecutive contour plots demonstrate how the talus perches on the posterior border of the osteotomy site and subsequently subluxates anteriorly over the ensuing 0.023 second.

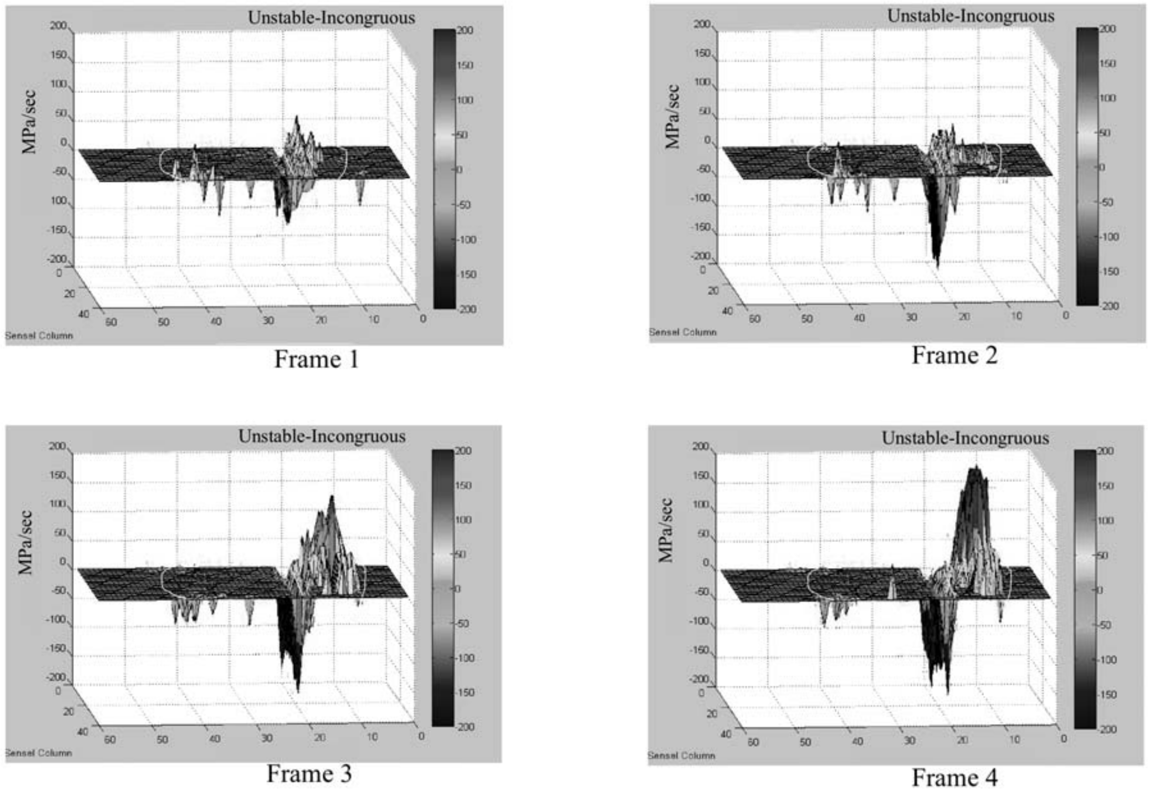

Fig. E2-B

Four consecutive contour plots of contact stress rates show that, as the talus subluxates anteriorly, it rapidly unloads the posterior border of the osteotomy site and rapidly loads the displaced fragment.